A process-based model for aeolian sediment transport and spatiotemporal varying sediment availability

Hoonhout, Bas; de Vries, Sierd

DOI
10.1002/2015JF003692

Publication date
2016

Published in
Journal of Geophysical Research: Earth Surface

AGU PUBLICATIONS

JGR

Journal of Geophysical Research: Earth Surface

RESEARCH ARTICLE
10.1002/2015JF003692

Key Points:
- A new process-based multifraction aeolian sediment transport model is presented
- The model simulates spatiotemporal variations in bed surface properties and sediment availability
- The model is first to account for effects of beach armoring on sediment availability

Supporting Information:
- Supporting Information S1

Correspondence to:
B. M. Hoonhout,
bas.hoonhout@deltares.nl

Citation:
Hoonhout, B. M. and S. de Vries (2016), A process-based model for aeolian sediment transport and spatiotemporal varying sediment availability, *J. Geophys. Res. Earth Surf.*, *121*, doi:10.1002/2015JF003692.

Received 14 AUG 2015
Accepted 7 AUG 2016
Accepted article online 22 AUG 2016

A process-based model for aeolian sediment transport and spatiotemporal varying sediment availability

Bas M. Hoonhout[1,2] and Sierd de Vries[1]

[1]Department of Hydraulic Engineering, Faculty of Civil Engineering and Geosciences, Delft University of Technology, Delft, Netherlands, [2]Unit of Hydraulic Engineering, Deltares, Delft, Netherlands

Abstract Aeolian sediment transport is influenced by a variety of bed surface properties, like moisture, shells, vegetation, and nonerodible elements. The bed surface properties influence aeolian sediment transport by changing the sediment transport capacity and/or the sediment availability. The effect of bed surface properties on the transport capacity and sediment availability is typically incorporated through the velocity threshold. This approach appears to be a critical limitation in existing aeolian sediment transport models for simulation of real-world cases with spatiotemporal variations in bed surface properties. This paper presents a new model approach for multifraction aeolian sediment transport in which sediment availability is simulated rather than parameterized through the velocity threshold. The model can cope with arbitrary spatiotemporal configurations of bed surface properties that either limit or enhance the sediment availability or sediment transport capacity. The performance of the model is illustrated using four prototype cases, the simulation of two wind tunnel experiments from literature and a sensitivity analysis of newly introduced parameters.

1. Introduction

Aeolian sediment transport is influenced by a variety of bed surface properties that are commonly found in coastal environments, like moisture, shells, strandlines, salt crusts, bed slopes, vegetation, nonerodible elements, and anthropogenic disturbances. The bed surface properties influence aeolian sediment transport by changing the sediment transport capacity and/or the sediment availability [*Kocurek and Lancaster*, 1999]. In current aeolian sediment transport models, the effects on the sediment transport capacity and sediment availability are generally incorporated through a single parameter: the velocity threshold. This approach appears to be a critical limitation in existing aeolian sediment transport models for simulation of real-world cases with spatiotemporal variations in bed surface properties.

The velocity threshold was introduced by *Bagnold* [1935] and incorporated in his initial aeolian sediment transport model [*Bagnold*, 1937] according to

$$\underbrace{q_{sat}}_{\substack{\text{sediment}\\\text{transport}\\\text{capacity}}} = \underbrace{\alpha C \frac{\rho_a}{g}\sqrt{\frac{d_n}{D_n}}}_{\substack{\text{properties of}\\\text{sediment in}\\\text{transport}}} \left(u_z - u_{th}\right)^3 \tag{1}$$

in which q_{sat} (kg/m/s) is the equilibrium or saturated sediment transport rate and represents the sediment transport capacity. The u_z (m/s) is the wind velocity at height z (m) and u_{th} the velocity threshold (m/s). The properties of the sediment in transport are represented by a series of parameters: C (-) is a parameter to account for the grain size distribution width, ρ_a (kg/m^3) is the density of the air, g (m/s^2) is the gravitational constant, d_n (m) is the nominal grain size, and D_n (m) is a reference grain size. α is a constant to account for the conversion of the measured wind velocity to the near-bed shear velocity following Prandtl-Von Kármán's Law of the Wall: $\left(\frac{\kappa}{\ln z/z'}\right)^3$ in which z' (m) is the height at which the idealized velocity profile reaches zero and κ (-) is the Von Kármán constant. Many studies following the work of *Bagnold* [1937] effectively proposed different parameterizations for sediment properties [e.g., *Owen*, 1964; *Hsu*, 1971; *Sørensen*, 2004] or changed the weight of the velocity threshold [e.g., *Kawamura*, 1951; *Lettau and Lettau*, 1978]. However, the characteristic structure and application of these models stayed essentially the same.

Sherman et al. [1998] and *Sherman and Li* [2012] summarized the performance of eight aeolian sediment transport models compared to field measurements on a sandy beach. All the models systematically overpredict the measured aeolian sediment transport rates, which is in agreement with other coastal field studies [e.g., *Jackson and Cooper*, 1999; *Lynch et al.*, 2008; *Davidson-Arnott and Bauer*, 2009; *Aagaard*, 2014]. Besides, the original model of *Bagnold* [1937] appeared to outperform the models of later date. In an attempt to explain the poor performance of aeolian sediment transport models in coastal environments, many authors emphasized the importance of bed surface properties. Typical bed surface properties that are found along the coast and assumed to explain at least partially the poor performance of aeolian sediment transport models are high moisture contents [e.g., *Wiggs et al.*, 2004; *Davidson-Arnott et al.*, 2008; *Darke and McKenna Neuman*, 2008; *McKenna Neuman and Sanderson*, 2008; *Udo et al.*, 2008; *Bauer et al.*, 2009; *Edwards and Namikas*, 2009; *Namikas et al.*, 2010; *Scheidt et al.*, 2010], salt crusts [e.g., *Nickling and Ecclestone*, 1981], bed slopes [e.g., *Iversen and Rasmussen*, 2006], vegetation [e.g., *Arens*, 1996; *Lancaster and Baas*, 1998; *Okin*, 2008; *Li et al.*, 2013; *Dupont et al.*, 2014], shell pavements [e.g., *van der Wal*, 1998; *McKenna Neuman et al.*, 2012], and sorted and armored beach surfaces [e.g., *Gillette and Stockton*, 1989; *Gillies et al.*, 2006; *Tan et al.*, 2013; *Cheng et al.*, 2015]. The influence of these bed surface properties on aeolian sediment transport has been investigated and often resulted in modified values for the velocity threshold [e.g., *Howard*, 1977; *Dyer*, 1986; *Belly*, 1964; *Johnson*, 1965; *Hotta et al.*, 1984; *Nickling and Ecclestone*, 1981; *Arens*, 1996; *King et al.*, 2005].

A critical limitation of the use of the velocity threshold alone to cope with the influence of bed surface properties is that it changes inherently in time and space [*Stout*, 2004] and that it accounts for two fundamentally different phenomena:

1. the change in the sediment transport capacity which represents the ease of sediment transport *over* a given bed; and
2. the change in sediment availability, which represents the ease of sediment entrainment *from* a given bed.

Although in uniform and constant situations, like often used in wind tunnel experiments, the difference might be negligible, in real-world field conditions it is not. The difference is most apparent when observing transport over a bed with spatial variations in bed surface properties. For example, due to tidal motions in the intertidal beach area, emergence of roughness elements in the dry beach area and vegetation in the dune area. In addition, temporal variations in bed surface properties, for example, due to tidal spring/neap cycles, rain showers, storm surges, seasonal variations in vegetation, and progressive armoring of the beach, increase the need for simulation rather than parameterization of bed surface properties and sediment availability (as discussed in section 2).

This paper presents a new model approach for aeolian sediment transport. The model simulates rather than parameterizes bed surface properties and sediment availability. The model explicitly defines sediment availability following *de Vries et al.* [2014a] and introduces multifraction aeolian sediment transport in order to simulate processes that limit the availability of sediment, like beach armoring and processes that enhance the availability of sediment, like hydraulic mixing. Consequently, the model can cope with arbitrary spatiotemporal configurations of bed surface properties. Although validation of the model is ongoing, the performance of the model is illustrated using four prototype cases, the simulation of two wind tunnel experiments from literature [*Nickling and McKenna Neuman*, 1995; *Dong et al.*, 2004a] and a sensitivity analysis of newly introduced parameters.

In literature the *velocity threshold* is used interchangeably to describe the (change in) sediment transport capacity and sediment availability. In this paper the term velocity threshold is strictly used to describe the (change in) sediment transport capacity (equation (1)). The term *sediment availability* is used in accordance with the terminology proposed by *Kocurek and Lancaster* [1999], which is often referred to as *sediment supply* in literature.

2. Model Challenges: Bed Surface Properties

The importance of spatiotemporal variations in bed surface properties for aeolian sediment transport is most apparent when observing transport over a bed consisting of both erodible and nonerodible fractions. Many studies have investigated the influence of varying grain sizes on aeolian sediment transport. In most cases it involved studies on the influence of nonerodible or roughness elements using either field experiments [e.g., *Davidson-Arnott et al.*, 1997; *Gillies et al.*, 2006; *Tan et al.*, 2013] or wind tunnel experiments

[e.g., *Gillette and Stockton*, 1989; *Nickling and McKenna Neuman*, 1995; *McKenna Neuman and Nickling*, 1995; *Dong et al.*, 2004a; *McKenna Neuman et al.*, 2012] and occasionally numerical modeling [e.g., *Turpin et al.*, 2010]. The studies typically use granular material with a clear bimodal distribution. A flat sandy surface is then partially covered by a significantly larger grain size fraction ranging from shells and gravel to pebbles and cobbles. Typically, the coverage of nonerodible elements is expressed using the roughness density λ as described by *Raupach et al.* [1993]. *Raupach et al.* [1993] uses the roughness density to determine the relative increase in the shear velocity threshold according to

$$R_t = \frac{u_{*th,S}}{u_{*th,R}} = \frac{1}{\sqrt{(1 - m\sigma\lambda)(1 + m\beta\lambda)}} \tag{2}$$

in which $u_{*th,S}$ is the shear velocity threshold with a bare surface, $u_{*th,R}$ is the shear velocity threshold with a surface including nonerodible elements, and m, σ, and β are calibration coefficients that account for the size and shape of the nonerodible elements.

2.1. Temporal Variations in Bed Surface Properties

The concept of the roughness density is useful to describe the instantaneous influence of roughness elements in the bed on aeolian sediment transport. However, it does not account for the fact that roughness elements tend to emerge from the bed over time due to winnowing of fines. Following *Gillette and Stockton* [1989], *Nickling and McKenna Neuman* [1995] and *McKenna Neuman and Nickling* [1995] showed that the winnowing of fines and the emergence of roughness elements result in a time-dependent aeolian sediment transport rate. The time dependency is caused by a recurrence relation between sediment transport and sediment availability. Consequently, neither the roughness density nor the sediment availability can be determined a priori. We argue that process-based simulation of bed surface properties rather than parameterization is needed to solve the instantaneous sediment availability.

McKenna Neuman et al. [2012] shows that even small shell fragments cause a sandy surface to be armored over time. But even in the absence of nonerodible roughness elements, spatiotemporal variations in bed surface properties may develop as the transport capacity is inversely related to the grain size [*Bagnold*, 1937] resulting in sediment sorting: a coarsening of the bed surface and downwind deposition of fines [*Bagnold*, 1937; *van der Wal*, 2000; *Arens et al.*, 2002].

2.2. Spatial Variations in Bed Surface Properties

Spatial variations in bed surface properties occur naturally in coastal environments. For example, strandlines locally cover the erodible bed and reduce the sediment availability. However, strandlines do not necessarily reduce the sediment transport capacity to the same extent and may even increase the transport capacity due to fully elastic collisions with the sediment in transport. The distinction between sediment availability and sediment transport capacity in relation to bed surface properties is not offered by existing models.

Dong et al. [2004a] describes a similar situation in a wind tunnel. In their experiment a patch of gravel (10–40 mm) is positioned downwind of a patch of sandy material. *Dong et al.* [2004a] show how the gravel patch reduces the aeolian sediment transport rate downwind of the domain compared to the situation without the gravel. However, in all conditions sediment passes the patch, while sediment availability from the patch is zero. There seems to be a tendency of an increase in sediment transport rate with increasing patch size when the patch size is relatively small. This is attributed to the change in transport characteristics due to fully elastic collisions between the sand grains and the gravel. Consequently, the saltation height and rebound angle increase and in turn influence the sediment transport capacity. Only for large patch sizes does the trapping of sand grains in the gravel pores become a dominant process resulting in a decrease in the sediment transport rate downwind of the gravel patch.

Dong et al. [2004a] acknowledged the limitations of the use of the shear velocity threshold to describe the results of his wind tunnel experiments. Therefore, they introduced a factor in the aeolian sediment transport formulation used that depends on the length of the gravel patch squared. Although an important observation, the method is hardly generalizable to more realistic situations where moist intertidal beaches are located adjacent to strandlines and armored beaches that subsequently border a vegetated dune. Therefore, to cope with spatially varying bed surface properties an aeolian sediment transport model is needed that provides a generic distinction between the effect of bed surface properties on the sediment transport capacity and sediment availability.

3. Model Concepts: Sediment Availability, Saturated Transport, and Entrainment

The sediment transport capacity and sediment availability together determine the sediment entrainment. Sediment availability differs from entrainment in that the availability defines the *potential* erosion of the bed, while the entrainment defines the *actual* erosion of the bed. If aeolian sediment transport is transport-limited, the sediment availability is larger than entrainment and not all available sediment will be transported. Consequently, entrainment is governed by the sediment transport capacity. If aeolian sediment transport is availability-limited, entrainment is equal to the sediment availability. Whether aeolian sediment transport is transport- or availability-limited depends on the balance between the sediment transport capacity and the sediment availability that are both influenced by bed surface properties. In the literature various concepts to incorporate the influence of bed surface properties in aeolian sediment transport models can be found:

1. the concept of the shear velocity threshold [e.g., *Howard*, 1977; *Dyer*, 1986; *Belly*, 1964; *Johnson*, 1965; *Hotta et al.*, 1984; *Nickling and Ecclestone*, 1981; *Arens*, 1996];
2. the concept of critical fetch [e.g., *Bauer and Davidson-Arnott*, 2002; *Delgado-Fernandez*, 2010]; and
3. the concept of explicit availability (or supply) [*de Vries et al.*, 2014a].

From these concepts the shear velocity threshold is typically applied in conjunction with a formulation for the aeolian sediment transport capacity (e.g., equation (1)). The sediment transport capacity described by these formulations is the equilibrium or saturated sediment transport rate. The saturated sediment transport rate is the maximum transport rate reached in case of a fetch (F) beyond the critical fetch (F_c) [*Bauer and Davidson-Arnott*, 2002]. In case of abundant sediment availability and fetches beyond the critical fetch the saturated sediment transport rate seems to be an appropriate indicator for the actual sediment flux downwind of the observed domain. However, in coastal environments fetches can be limited due to limited beach widths [e.g., *Jackson and Cooper*, 1999; *Bauer et al.*, 2009; *Davidson-Arnott et al.*, 2005; *Delgado-Fernandez*, 2010; *Dong et al.*, 2004b] and sediment availability is limited due to beach armoring as well as other bed surface properties. Consequently, in reality the saturated sediment transport rate is not necessarily an appropriate indicator for the sediment flux downwind of the observed domain.

The concept of critical fetch therefore introduces a measure to distinguish between saturated ($F \geq F_c$) and unsaturated sediment transport situations ($F < F_c$). In this approach the aeolian sediment transport rate, (critical) fetch distance, entrainment, and sediment availability are related following

$$q = \int_0^{\hat{F}} \phi(u_*, u_{*\mathrm{th}}, m_\mathrm{a})\mathrm{d}x \quad \text{with } \hat{F} = \min(F, F_c) \tag{3}$$

where q (kg/s/m) is the instantaneous sediment transport rate per unit width, F (m) is the fetch distance and F_c (m) the critical fetch distance, ϕ is the entrainment function that depends on the shear velocity u_* (m/s), the shear velocity threshold $u_{*\mathrm{th}}$ (m/s), and the available sediment mass m_a (kg/m^2). The parameter x (m) is the downwind distance from a zero-transport boundary. This integral is solved for by assuming a predefined entrainment rate. Equation (3) then simplifies to

$$q = \Phi(u_*, u_{*\mathrm{th}}, m_\mathrm{a}, \hat{F}) \tag{4}$$

where Φ is the analytically integrated solution to equation (3). *Delgado-Fernandez and Davidson-Arnott* [2011] use the critical fetch concept to incorporate the effect of spatiotemporal variations in soil moisture. However, due to the recurrence relation in time between the aeolian sediment transport rate q and the sediment availability m_a, neither the sediment availability nor the entrainment can be determined a priori and the integral in equation (3) cannot easily be solved analytically.

Equation (3) can be simplified by observing the difference between availability-limited and transport-limited situations. In availability-limited situations the entrainment function simplifies to $\frac{\partial m_\mathrm{a}}{\partial t}$, while in transport-limited situations the sediment availability is abundant. Equation (3) can therefore be rewritten as

$$q = \begin{cases} \int_0^{\hat{F}} \frac{\partial m_\mathrm{a}}{\partial t}\mathrm{d}x & \text{if availability-limited} \\ \int_0^{\hat{F}} \phi(u_*, u_{*\mathrm{th}})\mathrm{d}x & \text{if transport-limited} \end{cases} \tag{5}$$

The wind velocity can influence sediment availability indirectly through beach armoring. Given constant wind velocity, the development of a beach armor layer can turn a transport-limited situation into an availability-limited situation, which subsequently influences the instantaneous aeolian sediment transport

rate. In an availability-limited situation, entrainment does not depend on the wind velocity since the wind velocity is sufficiently high to mobilize all available sediment.

The distinction between availability-limited and transport-limited situations in equation (5) naturally reveals the fundamental difference between sediment availability and the sediment transport capacity and shows why these two phenomena cannot be represented by a single parameter like the shear velocity threshold. Moreover, equation (5) provides an opportunity to model availability-limited and transport-limited situations separately as proposed by *de Vries et al.* [2014a], who uses a 1-D advection formulation in combination with the concept of a spatiotemporal varying sediment availability m_a (or supply S_e according to the terminology of *de Vries et al.* [2014a])to regulate the entrainment, transport, and deposition of sediment by wind.

The disadvantage of the use of an explicit term for the sediment availability is that little is known about the quantitative relation between availability and the different availability-limiting bed surface properties. Moreover, also in the approach of *de Vries et al.* [2014a] sediment availability is not quantified by the model but is input to the model. Due to the recurrence relation between the sediment transport rate and sediment availability, the governing input parameter to this model is unknown and the resulting instantaneous sediment transport rate cannot be computed. Therefore, we propose to extend the approach of *de Vries et al.* [2014a] with numerical simulation of spatiotemporal varying bed surface properties and sediment availability.

4. Model Description

The model approach of *de Vries et al.* [2014a] is extended to compute the spatiotemporal varying sediment availability through simulation of the process of beach armoring. For this purpose the bed is discretized in horizontal grid cells and in vertical bed layers (2DV). Moreover, the grain size distribution is discretized into fractions. This allows the grain size distribution to vary both horizontally and vertically. A bed composition module is used to compute the sediment availability for each sediment fraction individually. This model approach is a generalization of existing model concepts, like the shear velocity threshold and critical fetch, and therefore compatible with these existing concepts.

4.1. Advection Scheme

A 1-D advection scheme is adopted in correspondence with *de Vries et al.* [2014a] in which c (kg/m^2) is the instantaneous sediment mass per unit area in transport:

$$\frac{\partial c}{\partial t} + u_z \frac{\partial c}{\partial x} = E - D \tag{6}$$

t (s) denotes time and x (m) denotes the cross-shore distance from a zero-transport boundary. E and D (kg/m^2/s) represent the erosion and deposition terms and hence combined represent the net entrainment of sediment. Note that equation (6) differs from Equation 9 in *de Vries et al.* [2014a] as they use the saltation height h (m) and the sediment concentration C_c (kg/m^3). As h is not solved for, the presented model computes the sediment mass per unit area $c = hC_c$ rather than the sediment concentration C_c. For conciseness we still refer to c as the *sediment concentration*.

The net entrainment is determined based on a balance between the equilibrium or saturated sediment concentration c_{sat} (kg/m^2) and the instantaneous sediment transport concentration c and is maximized by the available sediment in the bed m_a (kg/m^2) according to

$$E - D = \min\left(\frac{\partial m_a}{\partial t} \quad ; \quad \frac{c_{sat} - c}{T}\right) \tag{7}$$

T (s) represents an adaptation time scale that is assumed to be equal for both erosion and deposition. A time scale of 1 s is commonly used [*de Vries et al.*, 2014a].

The saturated sediment concentration c_{sat} is computed using an empirical sediment transport formulation (e.g., equation (1)) where the transport rate q_{sat} is divided by the wind velocity u_z to obtain a mass per unit area (per unit width):

$$c_{sat} = \max\left(0 \quad ; \quad \alpha C \frac{\rho_a}{g} \sqrt{\frac{d_n}{D_n}} \frac{\left(u_z - u_{th}\right)^3}{u_z}\right) \tag{8}$$

in which C (-) is an empirical constant to account for the grain size distribution width, ρ_a (kg/m^3) is the air density, g (m/s^2) is the gravitational constant, d_n (m) is the nominal grain size, D_n (m) is a reference grain size,

u_z (m/s) is the wind velocity at height z (m), and α (-) is a constant to convert from measured wind velocity to shear velocity.

Note that at this stage the spatial variations in wind velocity are not solved for, and hence, no morphological feedback is included in the simulation. The model is initially intended to provide accurate sediment fluxes from the beach to the dunes rather than to simulate subsequent dune formation.

4.2. Multifraction Erosion and Deposition

The formulation for the equilibrium or saturated sediment concentration c_{sat} (equation (8)) is capable of dealing with variations in grain size through the variables u_{th}, d_n, and C [*Bagnold*, 1937]. However, the transport formulation only describes the saturated sediment concentration assuming a fixed grain size distribution, but does not define how multiple fractions coexist in transport. If the saturated sediment concentration formulation would be applied to each fraction separately and summed up to a total transport, the total sediment transport would increase with the number of sediment fractions. Since this is unrealistic behavior the saturated sediment concentration c_{sat} for the different fractions should be weighted in order to obtain a realistic total sediment transport. Equation (7) therefore is modified to include a weighting factor $\hat{w}_k$ in which k represents the sediment fraction index:

$$E_k - D_k = \min\left(\frac{\partial m_{a,k}}{\partial t} \quad ; \quad \frac{\hat{w}_k \cdot c_{sat,k} - c_k}{T}\right) \tag{9}$$

It is common to use the grain size distribution in the bed as weighting factor for the saturated sediment concentration [e.g., *Delft3D-FLOW Manual*, 2014, section 11.6.4]. Using the grain size distribution at the bed surface as a weighting factor assumes, in case of erosion, that all sediment at the bed surface is equally exposed to the wind.

Using the grain size distribution at the bed surface as weighting factor in case of deposition would lead to the behavior where deposition becomes dependent on the bed composition. Alternatively, in case of deposition, the saturated sediment concentration can be weighted based on the grain size distribution in the air. Due to the nature of saltation, in which continuous interaction with the bed forms the saltation cascade, both the grain size distribution in the bed and in the air are likely to contribute to the interaction between sediment fractions. The ratio between both contributions in the model is determined by a bed interaction parameter ζ.

The weighting of erosion and deposition of individual fractions is computed according to

$$\hat{w}_k = \frac{w_k}{\sum_{k=1}^{n_k} w_k} \tag{10a}$$

$$\text{where} \quad w_k = (1-\zeta)\cdot w_k^{air} + (1-\hat{S}_k)\cdot w_k^{bed} \tag{10b}$$

in which k represents the sediment fraction index, n_k the total number of sediment fractions, w_k is the unnormalized weighting factor for fraction k, $\hat{w}_k$ is its normalized counterpart, w_k^{air} and w_k^{bed} are the weighting factors based on the grain size distribution in the air and bed, respectively, and $\hat{S}_k$ is the effective sediment saturation of the air. The weighting factors based on the grain size distribution in the air and the bed are computed using the following mass ratios:

$$w_k^{air} = \frac{c_k}{c_{sat,k}} \quad ; \quad w_k^{bed} = \frac{m_{a,k}}{\sum_{k=1}^{n_k} m_{a,k}} \tag{11}$$

The sum of the ratio w_k^{air} over the fractions denotes the degree of saturation of the air column for fraction k. The degree of saturation determines if erosion of a fraction may occur. Also, in saturated situations, erosion of a sediment fraction can occur due to an exchange of momentum between sediment fractions, which is represented by the bed interaction parameter ζ. The effective degree of saturation is therefore also influenced by the bed interaction parameter and defined as

$$\hat{S}_k = \min\left(1 \quad ; \quad (1-\zeta)\cdot\sum_{k=1}^{n_k} w_k^{air}\right) \tag{12}$$

When the effective saturation is greater than or equal to unity, the air is (over)saturated and no erosion will occur. The grain size distribution in the bed is consequently less relevant and the second term in equation (10)

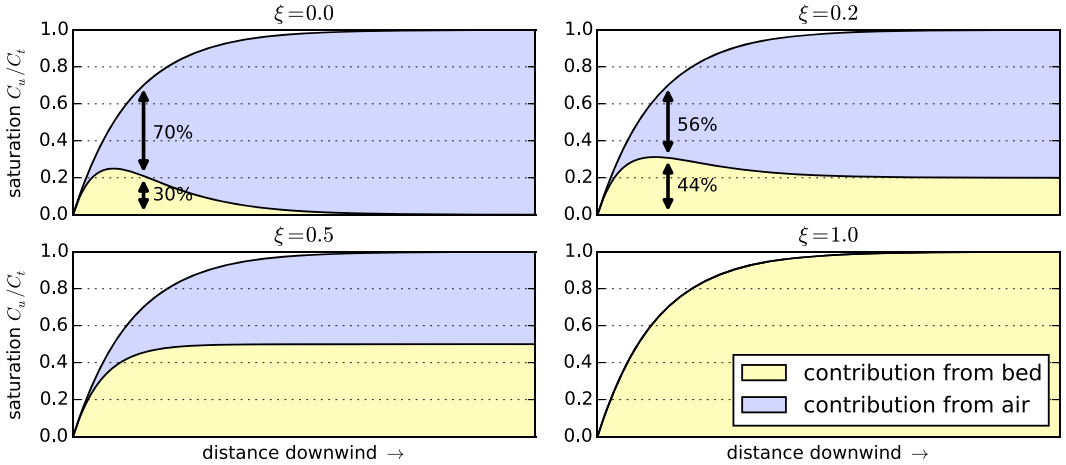

Figure 1. Contributions of the grain size distribution in the bed and in the air to the weighting factors $\hat{w}_k$ for the equilibrium sediment concentration in equation (9) for different values of the bed interaction parameter.

is thus minimized and zero in case $\zeta = 0$. In case the effective saturation is less than unity erosion may occur and the grain size distribution of the bed also contributes to the weighting over the sediment fractions. The weighting factors for erosion are then composed from both the grain size distribution in the air and the grain size distribution at the bed surface. Finally, the resulting weighting factors are normalized to sum to unity over all fractions ($\hat{w}_k$).

The composition of weighting factors for erosion is based on the saturation of the air column. The nonsaturated fraction determines the potential erosion of the bed. Therefore, the nonsaturated fraction can be used to scale the grain size distribution in the bed in order to combine it with the grain size distribution in the air according to equation (10). The nonsaturated fraction of the air column that can be used for scaling is therefore $1 - \hat{S}_k$.

For example, if bed interaction is disabled ($\zeta = 0$) and the air is 70% saturated, then the grain size distribution in the air contributes 70% to the weighting factors for erosion, while the grain size distribution in the bed contributes the other 30% (Figure 1, top left). In case of (over)saturation the grain size distribution in transport contributes 100% to the weighting factors and the grain size distribution in the bed is of no influence. Transport progresses in downwind direction without interaction with the bed.

To allow for bed interaction in saturated situations in which no net erosion can occur, the bed interaction parameter ζ is used (Figure 1). The bed interaction parameter can take values between 0.0 and 1.0 in which the weighting factors for the equilibrium or saturated sediment concentration in an (over)saturated situation are fully determined by the grain size distribution in the bed or in the air, respectively. A bed interaction value of 0.2 represents the situation in which the grain size distribution at the bed surface contributes 20% to the weighting of the saturated sediment concentration over the fractions. In the example situation, where the air is 70% saturated, such value for the bed interaction parameter would lead to weighting factors that are constituted for $70\% \cdot (100\% - 20\%) = 56\%$ based on the grain size distribution in the air and for the other 44% based on the grain size distribution at the bed surface (Figure 1, top right).

The parameterization of the exchange of momentum between sediment fractions is an aspect of saltation that is still poorly understood. Therefore, calibration of the bed interaction parameter ζ is necessary. The model parameters in equation (8) can be chosen in accordance with the assumptions underlying multifraction sediment transport. C should be set to 1.5 as each individual sediment fraction is well sorted, d_n should be chosen equal to D_n as the grain size dependency is implemented through u_{th}. The parameter u_{th} typically varies between 1 and 6 m/s for sand.

4.3. Simulation of Sediment Sorting and Beach Armoring

Since the equilibrium or saturated sediment concentration $c_{sat,k}$ is weighted over multiple sediment fractions in the extended advection model, also the instantaneous sediment concentration c_k is computed for each sediment fraction individually. Consequently, grain size distributions may vary over the model domain and in time. These variations are thereby not limited to the horizontal but may also vary over the vertical since

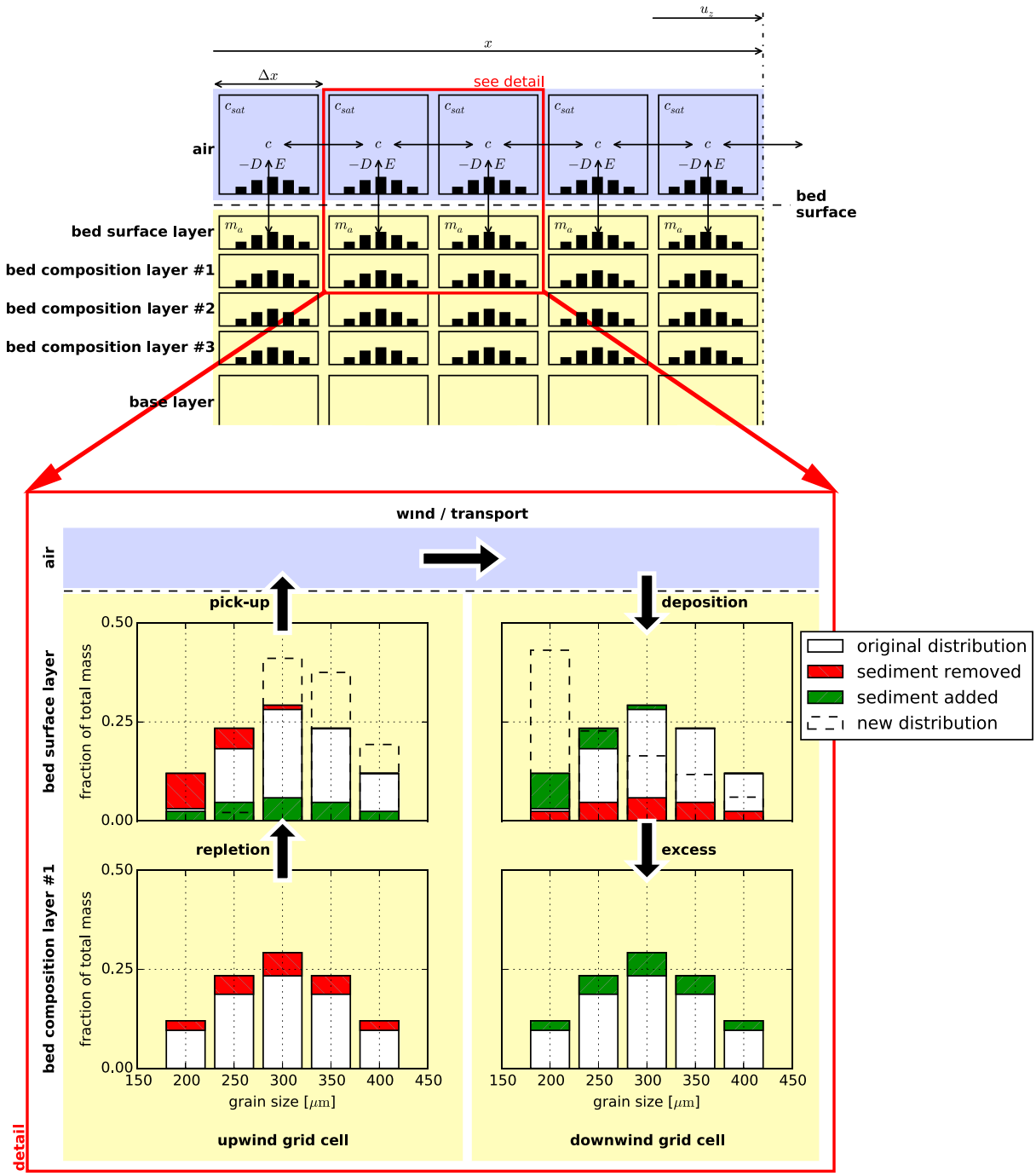

Figure 2. Schematic of bed composition discretization and advection scheme. Horizontal exchange of sediment may occur solely through the air that interacts with the *bed surface layer*. The detail presents the simulation of sorting and beach armoring where the bed surface layer in the upwind grid cell becomes coarser due to nonuniform erosion over the sediment fractions, while the bed surface layer in the downwind grid cell becomes finer due to nonuniform deposition over the sediment fractions. Symbols refer to equations (6) and (7).

fine sediment may be deposited on top of coarse sediment or, reversely, fines may be eroded from the bed surface leaving coarse sediment to reside on top of the original mixed sediment. In order to allow the model to simulate the processes of sediment sorting and beach armoring the bed is discretized in horizontal grid cells and vertical bed layers (2DV; Figure 2).

The discretization of the bed consists of a minimum of three vertical bed layers with a constant thickness and an unlimited number of horizontal grid cells. The top layer is the *bed surface layer* and is the only layer

that interacts with the wind and hence determines the spatiotemporal varying sediment availability and the contribution of the grain size distribution in the bed to the weighting of the saturated sediment concentration. One or more *bed composition layers* are located underneath the bed surface layer and form the upper part of the erodible bed. The bottom layer is the *base layer* and contains an infinite amount of erodible sediment according to the initial grain size distribution. The base layer cannot be eroded but can supply sediment to the other layers.

Each layer in each grid cell describes a grain size distribution over a predefined number of sediment fractions (Figure 2, detail). Sediment may enter or leave a grid cell only through the bed surface layer. Since the velocity threshold depends among others on the grain size, erosion from the bed surface layer will not be uniform over all sediment fractions, but will tend to erode fines more easily than coarse sediment (Figure 2, detail, top left). If sediment is eroded from the bed surface layer, the layer is repleted by sediment from the lower bed composition layers. The repleted sediment has a different grain size distribution than the sediment eroded from the bed surface layer. If more fines are removed from the bed surface layer in a grid cell than repleted, the median grain size increases. If erosion of fines continues, the bed surface layer becomes increasingly coarse. Deposition of fines or erosion of coarse material may resume the erosion of fines from the bed.

In case of deposition the process is similar. Sediment is deposited in the bed surface layer that then passes its excess sediment to the lower bed layers (Figure 2, detail, top right). If more fines are deposited than passed to the lower bed layers, the bed surface layer becomes increasingly fine.

4.4. Simulation of the Emergence of Nonerodible Roughness Elements

Sediment sorting may lead to the emergence of nonerodible elements from the bed. Nonerodible roughness elements may shelter the erodible bed from wind erosion due to shear partitioning, resulting in a reduced sediment availability [*Raupach et al.*, 1993]. Therefore, equation (2) is implemented according to

$$u_{*\mathrm{th},R} = u_{*\mathrm{th}} \cdot \sqrt{\left(1 - m \cdot \sum_{k=k_0}^{n_k} w_k^{\mathrm{bed}}\right)\left(1 + \frac{m\beta}{\sigma} \cdot \sum_{k=k_0}^{n_k} w_k^{\mathrm{bed}}\right)} \tag{13}$$

in which σ is the ratio between the frontal area and the basal area of the roughness elements and β is the ratio between the drag coefficients of the roughness elements and the bed without roughness elements. The parameter m is a factor to account for the difference between the mean and maximum shear stress and is usually chosen as 1.0 in wind tunnel experiments and may be lowered to 0.5 for field applications. The roughness density λ in the original equation of *Raupach et al.* [1993, equation (2)] is obtained from the mass fraction in the bed surface layer w_k^{bed} (equation (11)) according to

$$\lambda = \frac{\sum_{k=k_0}^{n_k} w_k^{\mathrm{bed}}}{\sigma} \tag{14}$$

in which k_0 is the index of the smallest nonerodible sediment fraction in current conditions and n_k is the total number of sediment fractions. It is assumed that the sediment fractions are ordered by increasing size. Whether a fraction is erodible depends on the sediment transport capacity.

4.5. Simulation of the Hydraulic Mixing, Infiltration, and Evaporation

As sediment sorting due to aeolian processes can lead to armoring of a beach surface, mixing of the beach surface, or erosion of coarse material may undo the effects of armoring. To ensure a proper balance between processes that limit and enhance sediment availability in the model both types of processes need to be sufficiently represented when simulating spatiotemporal varying bed surface properties and sediment availability.

A typical upwind boundary in coastal environments during onshore winds is the water line. For aeolian sediment transport the water line is a zero-transport boundary. In the presence of tides, the intertidal beach is flooded periodically. Hydraulic processes like wave breaking mix the bed surface layer of the intertidal beach, break the beach armoring, and thereby influence the availability of sediment. Moreover, the hydraulic processes periodically wet the intertidal beach temporally increasing the shear velocity threshold. Infiltration and evaporation subsequently dry the beach.

In the model the mixing of sediment is simulated by averaging the sediment distribution over the depth of disturbance (Δz_d). The depth of disturbance is linearly related to the breaker height [e.g., *King*, 1951; *Williams*,

1971; *Masselink et al.*, 2007]. *Masselink et al.* [2007] proposes an empirical factor $f_{\Delta z_d}$ (-) that relates the depth of disturbance directly to the local breaker height according to

$$\Delta z_d = f_{\Delta z_d} \cdot \min(H \quad ; \quad \gamma \cdot d) \tag{15}$$

in which the offshore wave height H (m) is taken as the local wave height maximized by a maximum wave height over depth ratio γ (-). The parameter d (m) is the water depth that is provided to the model through an input time series of water levels. Typical values for $f_{\Delta z_d}$ are 0.05 to 0.4 and 0.5 for γ.

The drying of the beach is simulated by simplified functions for infiltration and evaporation. Infiltration is represented by an exponential decay function that is governed by a drying time scale T_{dry}. Evaporation is simulated using an adapted version of the Penman-Monteith equation [*Shuttleworth*, 1993] that is governed by meteorological time series of solar radiation, temperature, and humidity.

5. Results

The model is applied to a series of prototype cases to illustrate the processes described by the model, two wind tunnel experiments to illustrate the capabilities of the model to simulate spatiotemporal variations in bed surface properties and sediment availability and a sensitivity analysis.

5.1. Prototype Cases

The four prototype cases P1 to P4 are intended to illustrate the capabilities of the presented model to simulate processes of sediment sorting [*van der Wal*, 2000; *Arens et al.*, 2002] and beach armoring [*van der Wal*, 1998]. The prototype cases are constructed using a 120 m schematized linear beach with a 1:20 slope, a wind velocity of 12 or 30 m/s, a drying time scale T_{dry} of 3 h, constant evaporation, and a simulation time of 30 days. The prototype cases are initialized with lognormally distributed sediment with $d_{50} = 335$ μm ($\Phi - \text{scale} = 1.6$, $\sigma_\Phi = 0.4$), which is representative for nourished poorly sorted beaches along the Dutch coast. Parameterizations for shells and shell fragments in equation (13) are based on experiments described by *McKenna Neuman et al.* [2012] and chosen as $m = 0.5$, $\sigma = 4.2$, and $\beta = 130$. The four scenarios described by the prototype cases are

1. This scenario is used as reference for normalization and involves sand only and no tidal movement. The model is forced by a constant wind of 12 m/s. Sediment sorting occurs due to the presence of a wide range of sediment fractions. However, beach armoring does not occur due to the absence of shells, resulting in an almost constant sediment transport rate at the downwind end of the domain.
2. This scenario involves 5% of shells and shell fragments ranging from 2 to 30 mm and no tidal movement. The model is forced by a constant wind of 12 m/s. The presence of shells means that beach armoring occurs that causes spatiotemporal variations in sediment availability and a decrease in sediment transport.
3. This scenario involves 5% of shells and shell fragments and a sinusoidal tide with a 2 m tidal range and a tidal period of 12 h. The tide periodically floods a 40 m intertidal beach area. The model is forced by a constant wind of 12 m/s. The tidal movement causes mixing of the bed surface layer in the intertidal beach area reducing the effects of beach armoring.
4. This scenario is equal to scenario P3, but the model is forced by a wind of 12 m/s that is increased twice to 30 m/s to simulate the effect of higher energy wind events that (partially) reset the composition of the bed surface layer and temporarily increase the sediment availability in the dry beach area.

Figure 3 presents the simulated aeolian sediment transport rates at the downwind end of the domain for cases P2 to P4 over the course of 30 days of simulation time. The results are normalized using the transport rate in case P1. The reference case P1 shows an almost constant transport rate over the entire course of the simulation. The presence of shells in case P2 results in a reduction of sediment availability. As a result, the transport rates in case P2 are lower compared to case P1. The transport rate decreases as more shells emerge from the bed and a beach armor layer develops. In case P2 there are no processes that break the armoring, and the transport rates asymptotically reach zero. The beach armor layer develops in the direction of the wind. Therefore, the relative contribution of the downwind part of the beach ($x \geq 40$) to the total sediment transport increases over time.

Case P3 includes tidal movement and hydraulic mixing. At the high water line the sediment transport is zero during high tide and maximized during low tide. Initially, transport is not saturated at the high water line and entrainment of sediment continues over the dry beach. As shells emerge from the bed, a beach armor

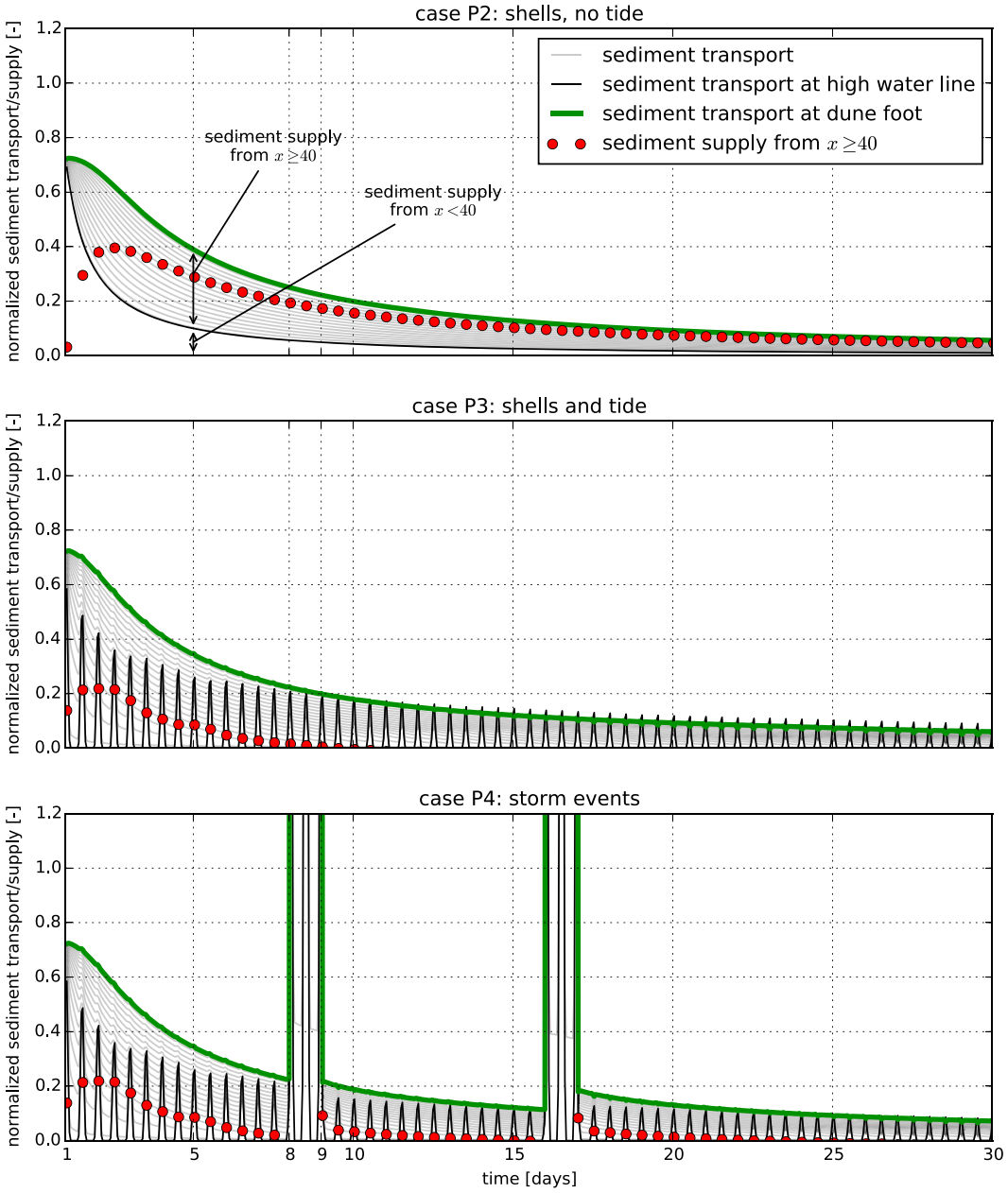

Figure 3. Sediment transport in time and over the model domain for three scenarios with constant wind. Each line depicts a different location along the beach, starting from $x = 40$ m, which coincides with the high water line in cases P3 and P4, and ends at the dune foot. Results are normalized using the transport rate in case P1 with almost constant transport (not shown). The difference between the sediment transport at dune foot (green) and the sediment transport at $x = 40$ m is visualized by the red dots and represents the sediment supply from the dry beach. In cases P3 and P4 the sediment transport at the high water line periodically exceeds the sediment transport at the dune foot, indicating local deposition of sediments originating from the intertidal beach.

layer develops that reduces sediment availability. The reduction of sediment availability progresses slower at the intertidal beach compared to the dry beach due to hydraulic mixing. After 8 days the sediment transport rates at the high water line start to exceed the sediment transport rates at the dune foot during low water. Sediment that is eroded from the intertidal beach during low water is partially trapped at the dry beach due to differences in roughness. During subsequent high water, when the sediment supply from the intertidal beach ceases, these deposits are again entrained and blown downwind. The net erosion from the dry beach ultimately approaches zero as armoring of the dry beach progresses. At this point all sediment deposited downwind originates directly from the intertidal beach. However, due to the spatial differences in roughness,

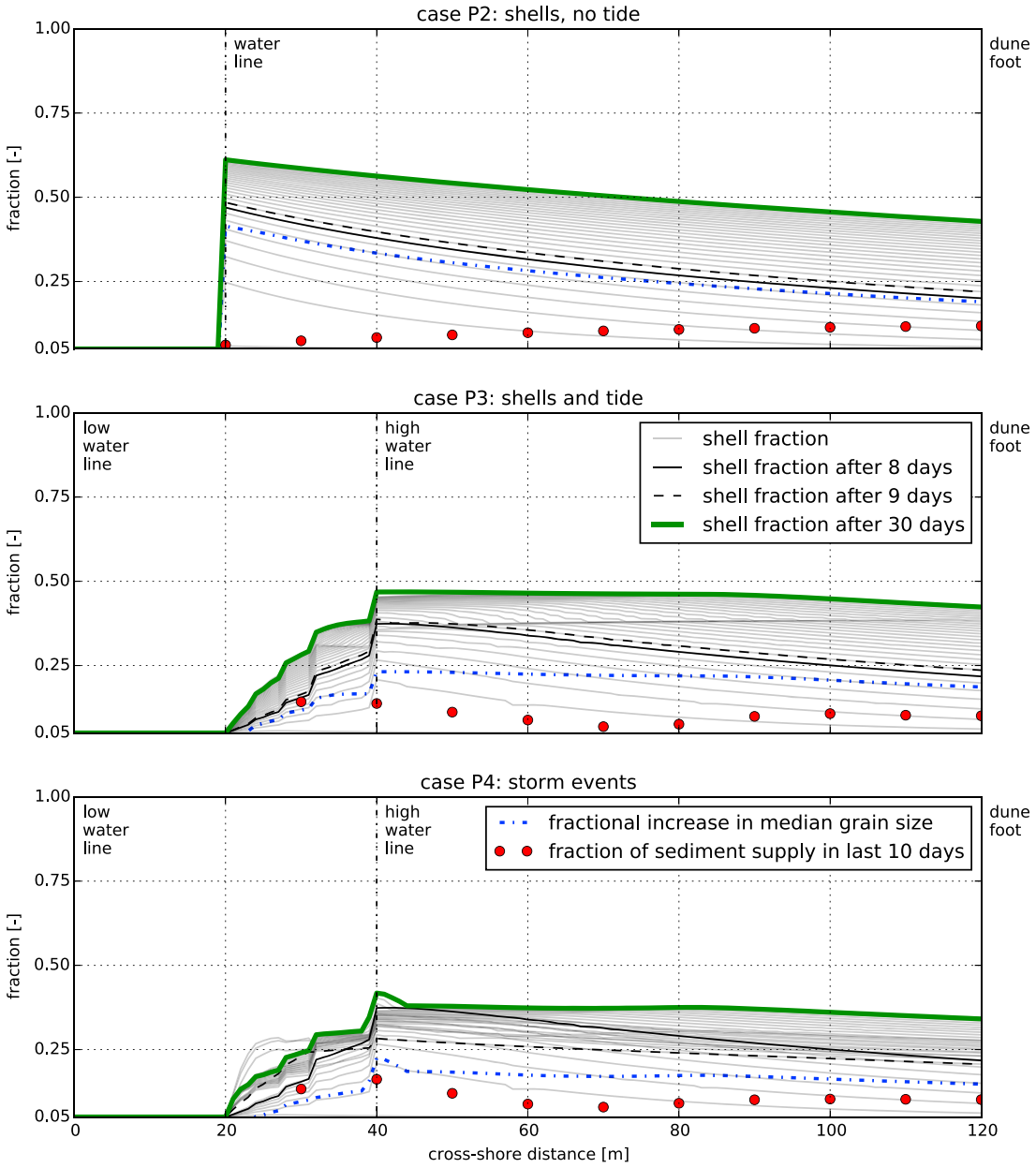

Figure 4. Distribution of the shell fraction over the model domain and in time. Sediment supply is inversely related to the degree of beach armoring, indicated by the shell fraction. Median grain size increases with the increase in shell fraction indicating erosion of predominantly fines. High-energy wind events in case P4 even mobilize shell fractions resulting in a decrease in beach armoring and an increase in sediment availability.

sediment is temporally deposited at the dry beach and cause the sediment transport rates at the dune foot to be only weakly correlated with the tidal movement.

Case P4 shows a pattern similar to case P3, but after 8 and 16 days a relatively high-energy wind event passes for 24 h. As a result, the transport rate spikes, but an elevated transport rate is also visible after the wind velocity drops. During the high-energy wind event even small shell fragments are mobilized. The beach armoring is therefore (partially) removed and more sediment is available for transportation afterward. This leads to a prolonged peak in sediment transport and an increase of the relative contribution of the dry beach to the total sediment transport at the dune foot. After the beach armoring is reestablished over time the transport rates approach the rates of case P3 again.

The differences in transport rate between the prototype cases are directly related to sediment availability, since the wind is constant in all cases but case P4. Figure 4 shows the fractions of shells and shell fragments

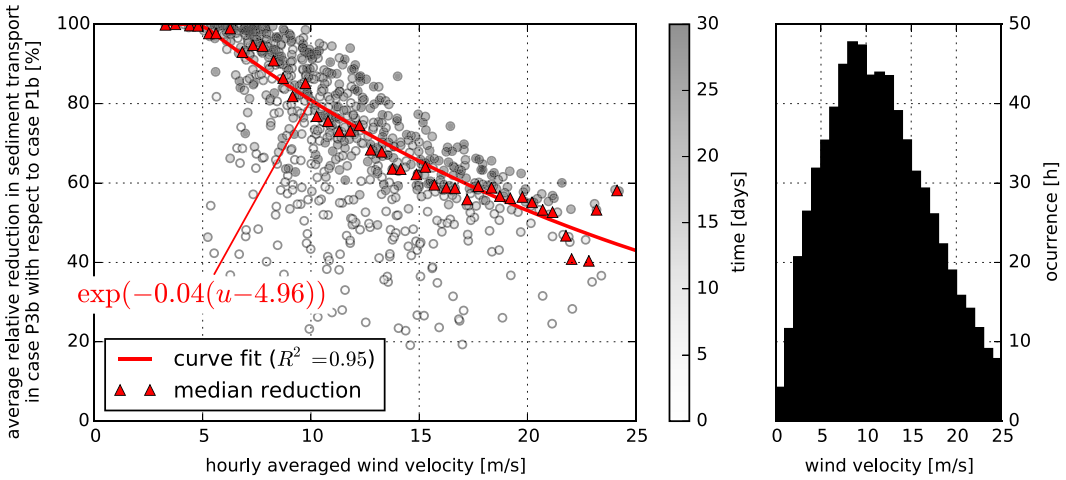

Figure 5. (left) Average reduction in sediment transport in prototype case P3b compared to case P1b depending on the hourly averaged wind velocity. (right) The results are obtained using a synthetic variable wind time series following a Weibull distribution with a mean wind velocity of 12 m/s. The sediment transport reduction (scatter) is binned according to the wind velocity using 0.5 m/s bins. The median reduction per bin (triangles) is used to fit an exponential curve (line). The reduction tends to increase during the simulation (scatter colors).

in the bed surface layer for case P2 to P4. The shell fraction increases over time in all simulations. In case P2 the shell fraction peaks at the water line as the beach armor layer develops in downwind direction. Consequently, at the end of the simulation most sediment originates from the downwind end of the beach where the beach armoring is least developed. In cases P3 and P4 hydraulic mixing causes the shell fraction in the intertidal beach to remain low, resulting in a different distribution of shells compared to case P2 and hence a difference in sediment availability. Consequently, at the end of the simulation most sediment originates from the intertidal beach. In reality, the contribution of the intertidal beach to the total sediment transport is likely to be higher as more marine processes counteract the local development of a beach armor layer than currently simulated, like marine deposits and buoyancy of shells. In case P4 the drop in shell fraction from days 8 to 9 is related to the first high-energy wind event. At the end of the simulation, the fraction of sediment that originates from the intertidal beach is relatively low compared to case P3. In all cases also the median grain size in the bed surface layer increases, indicating that predominantly fine sediment is eroded from the bed. The unbalanced sediment transport over the fractions cause sediment sorting in downwind direction.

The contribution to the instantaneous sediment transport of the specific processes described by the model can be distinguished in the prototype cases P1 to P4, because a constant wind velocity is imposed. If a more realistic variable wind velocity time series is used, the contributions of the specific processes are obscured by the wind-related variance. To show that the simulation of spatiotemporal bed surface properties and sediment are also important in variable wind conditions, prototype cases P1 to P3 are repeated using a synthetic variable wind time series (P1b to P3b). The time series is generated using a Markov Chain Monte Carlo (MCMC) simulation following a Weibull distribution with a mean wind velocity of 12 m/s.

Figure 5 shows the sediment transport rate in case P3b normalized by the sediment transport rate in case P1b depending on the hourly averaged wind velocity. To remove the influence of the wind variability, the normalized sediment transport time series obtained from the simulations are binned according to the hourly averaged wind velocity in 0.5 m/s bins. The median transport rate in each bin is subsequently determined to obtain a relation between instantaneous normalized sediment transport and wind velocity. The reduction is close to 100% up to wind velocities of 5 m/s and subsequently decreases according to an exponential function. The median reduction for 12 m/s wind velocity is 74%, which is less than the maximum reduction of 95.0% with a constant 12 m/s wind velocity in case P3. The reduction tends to increase during the simulation as beach armoring progresses.

5.2. Wind Tunnel Experiments

To illustrate the applicability of the model approach, two unrelated wind tunnel experiments obtained from literature are simulated that involve either temporal [*Nickling and McKenna Neuman*, 1995] or spatial [*Dong et al.*, 2004a] variations in bed surface properties as discussed in section 2.

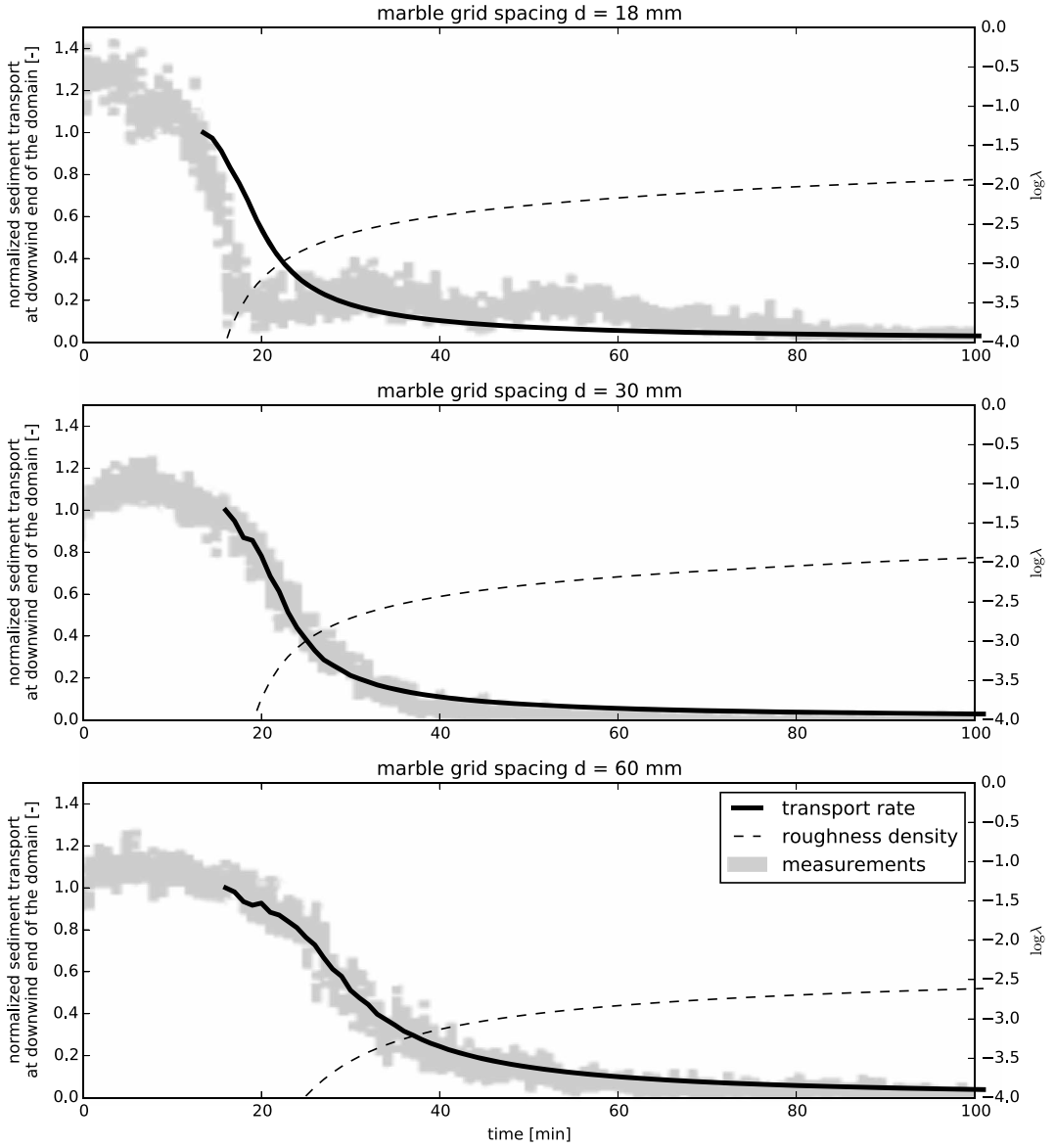

Figure 6. Comparison between modeled and measured normalized sediment transport rates from wind tunnel experiments described in *Nickling and McKenna Neuman* [1995]. The dashed line depicts the emergence of marbles in terms of increasing roughness density. The visualization of the measurement results is copied from Figure 4 in the original publication without digitization.

Nickling and McKenna Neuman [1995] describe an experiment in a wind tunnel with a 4.5 m working section in which a grid of 18 mm marbles was buried in sandy material with $d_{50} = 270$ μm. During the experiment with constant wind of 8 m/s, measured at 25 cm above the bed, the sand is winnowed from in between the marbles resulting in the emergence of the marbles over time. The emergence of the marbles cause the bed to become armored. The effect of armoring of a marble extends beyond the marble dimensions due to shadowing effects in the lee of the marble described by equation (13). All parameter values, including z', are obtained from *Nickling and McKenna Neuman* [1995], and hence, no further calibration of parameters is performed for this simulation.

Figure 6 shows the modeled normalized sediment transport rate in comparison with the measurements described in *Nickling and McKenna Neuman* [1995]. Where the measurements start with a relatively constant transport and even a slight increase in transport, the model predicts an immediate decrease in transport. The marbles are modeled as a large sediment fraction for which its presence in a bed composition layer is

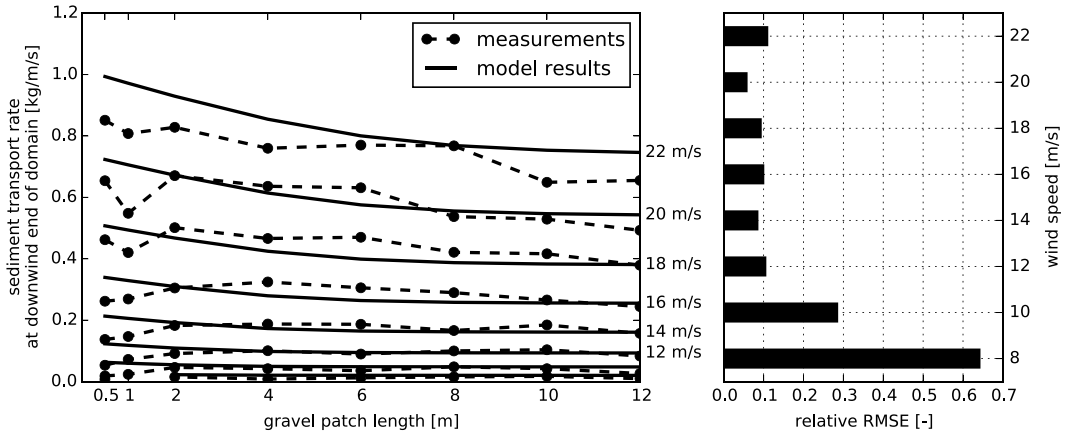

Figure 7. Comparison between (left) model results and measurements from wind tunnel experiments described in *Dong et al.* [2004a] and (right) RMS errors relative to the mean measured transport rate. The measured transport rates with a wind velocity of 22 m/s are underestimated due to surpassing of sediment over the sediment trap [*Dong et al.*, 2004a].

described by a mass fraction rather than a location. Therefore, it is possible to define the marble density but not the exact marble locations. Consequently, from the start of the simulation marbles start to emerge from the bed resulting in an immediate decrease in sediment transport. In contrast, in the wind tunnel the marbles are covered with a thin layer of sand that was removed first before the marbles start to emerge. The initial emergence of the marbles coincided with a slight increase in sediment transport. *Nickling and McKenna Neuman* [1995] attributes this rise to a pronounced change in boundary conditions and turbulence. Since these small-scale variations in the wind shear are not represented in the model, the rise in transport is not visible in the model results. However, the decrease in sediment transport due to the emergence of the marbles for the three different grid spacings described in *Nickling and McKenna Neuman* [1995] is qualitatively represented by the model.

Dong et al. [2004a] describe an experiment in a wind tunnel with a 21 m working section in which a patch of gravel with diameter 10–40 mm was positioned downwind of a sandy bed with $d_{50} = 180$ µm. The length of the gravel patch was varied between the experiments from 0.5 to 12 m and the wind velocity from 8 to 22 m/s, measured at 60 cm above the bed. The free-flow wind velocities are converted to shear velocities assuming $z' = 6$ mm. The gravel patch traps saltating grains. In the model the entrapment of grains is simulated as an exchange of momentum between the sandy fractions and the immobile gravel fraction. This exchange is governed by the bed interaction parameter, which is calibrated for this simulation and found to be 0.05.

Figure 7 shows the modeled sediment transport rate in comparison with the measurements described in *Dong et al.* [2004a]. The increase in sediment transport with increasing wind velocity is well represented by the model given the uniform RMSE among the different wind velocities. The decrease in sediment transport rate with increasing gravel patch length is represented by the model with a relative RMSE of less than 10% for all except the lowest and highest wind velocities. Significant surpassing of sediment over the sediment trap during the measurements with 22 m/s wind velocity is reported by *Dong et al.* [2004a], which explains the consistent overprediction of the sediment fluxes by the model. The discrepancy between the model and the measurements for the 8 and 10 m/s wind velocities is less consistent and is expected to be a result of a low signal-to-noise ratio related to the small sediment fluxes. Also, for short gravel patch lengths the model deviates from the measurements. The relatively high variability over the 0.5 to 2 m gravel patch lengths is attributed to a change in transport characteristics [*Dong et al.*, 2004a] due to fully elastic collisions between the sand grains and the gravel. A bed interaction parameter that is not constant is needed to capture this behavior in the model.

5.3. Sensitivity

The sensitivity of the model to four newly introduced parameters and the wind velocity is determined to obtain insight in the importance of these parameters to the model results. The newly introduced parameters are the bed interaction parameter, depth of disturbance factor, the drying time scale, and the grain size

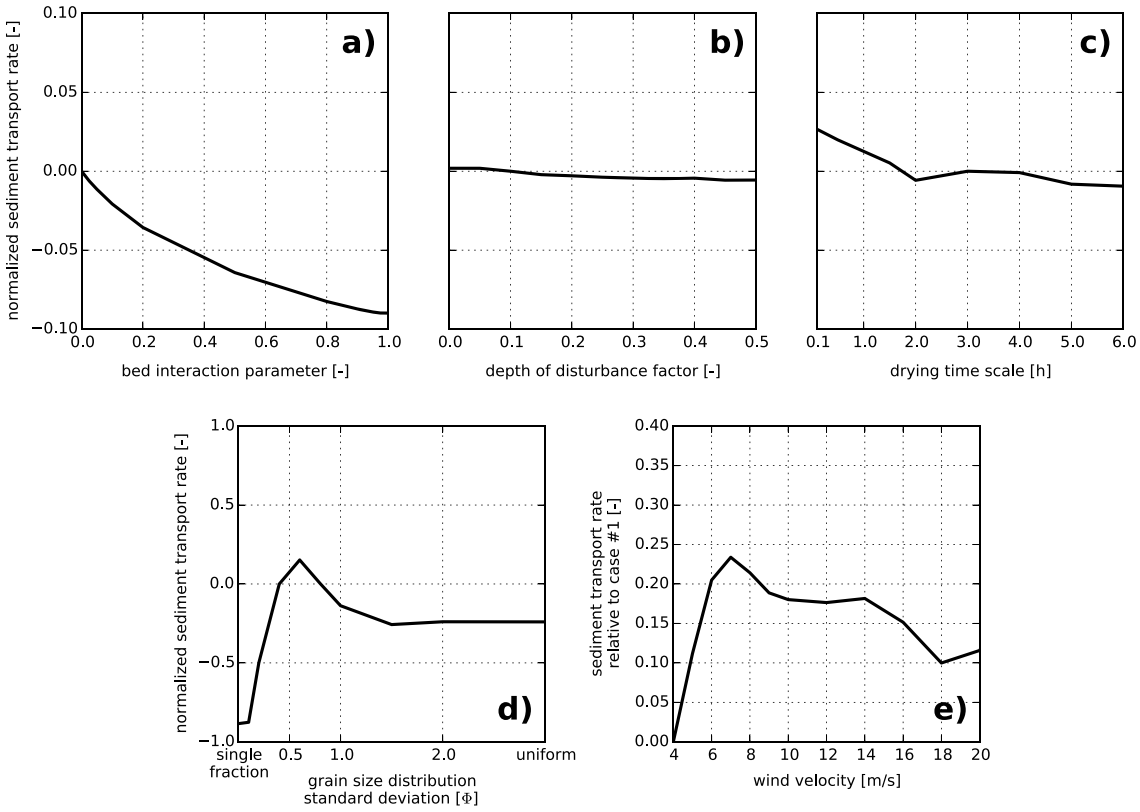

Figure 8. Sensitivity of the total normalized sediment transport with respect to case P3 for (a–d) four newly introduced parameters and (e) the wind velocity. The sensitivity of the wind velocity is expressed with respect to the transport rate in case P1.

distribution standard deviation. Case P3 as presented in section 5.1 is used as starting point for the sensitivity analysis. Figure 8 shows the change in normalized total sediment transport given variations of each of the four model parameters and the wind velocity.

The bed interaction parameter, the depth of disturbance factor, and the drying time scale affect the source area of aeolian sediment (Figures 8a–8c). In the absence of bed interaction all sediment entrained in the intertidal beach area is being transported to the downwind end of the domain, unhindered. In contrast, in the presence of bed interaction sediment from the intertidal beach area may be trapped in the beach armor layer that is being developed in the dry beach area during the simulation. Consequently, the total sediment transport reduces with increasing bed interaction. The bed interaction parameter parameterizes the exchange between sediment fractions, which is an aspect of saltation that is still poorly understood. In particular situations with a large spatial variability in bed surface properties, the bed interaction parameter is expected to show a more significant sensitivity [e.g., *Dong et al.*, 2004a]. Therefore, calibration of the bed interaction parameter is necessary in such situations.

The depth of disturbance factor shows no significant sensitivity as aeolian sediment supply from the intertidal beach is concentrated close to the water line where wave heights are negligible. Lower parts of the intertidal beach are continuously too moist for sediment to be entrained. The sensitivity to the depth of disturbance factor increases with decreasing drying time scale, but typically only for values smaller than 0.5 m. The sensitivity to the drying time scale shows that for time scales larger than several hours the intertidal beach is continuously too moist for sediment to be entrained. For small drying time scales the intertidal beach supplies aeolian sediment that contains relatively many fines.

From the sensitivity of the grain size distribution width, represented by the grain size distribution standard deviation and strictly speaking not a model parameter, it can be concluded that the introduction of multiple sediment fractions has a significant impact on the sediment transport rate (Figure 8d). However, for poorly sorted sediments the sensitivity of the model to the distribution width is limited. Beyond a standard deviation of $\sigma_\Phi = 1.5$ the development of the sediment rate is similar to the transport rate with a uniform distribution.

The rate of armoring depends on the presence of nonerodible sediment fractions. Whether a sediment fraction is erodible depends on the wind transport capacity. Therefore, the rate of armoring and consequently the instantaneous sediment availability depends on the wind velocity. Figure 8e depicts the sediment transport rate in case P3 with respect to the almost constant transport rate in case P1 for different wind velocities. For low wind velocities all shell fractions can contribute to the establishment of a beach armor layer, but the beach armor layer develops slowly as the winnowing of fines is dependent on the entrainment rate. For high wind velocities even shell fragments may be mobilized, but the beach armor layer consisting of larger shells is developed quickly. Consequently, the reduction of sediment transport is present over all wind velocities and 83% on average.

6. Discussion

Process-based simulation of bed surface properties and sediment supply provides an alternative for complex spatiotemporal parameterizations. Nevertheless, process-based simulation itself requires parameterization, calibration, and validation. These parameterizations are generally less complex as they describe static properties rather than spatiotemporal varying processes.

6.1. Parameterization

Compared to existing models for availability-limited aeolian sediment transport, the need for complex parameterization has been reduced in the presented model. The adoption of the advection model of *de Vries et al.* [2014a] makes parameterization of spatiotemporal variations in the shear velocity threshold, like those attempted by *Nickling and McKenna Neuman* [1995], *Dong et al.* [2004a], and others, unnecessary. In addition, process-based simulation of bed surface properties makes parameterization of the inherently time-varying sediment availability m_a unnecessary. Existing parameterizations for the shear velocity threshold under influence of moisture, vegetation, sediment sorting, and other bed surface properties are still valid for the instantaneous shear velocity threshold.

Despite the efforts to minimize complex parameterizations that are difficult to generalize, the model also introduces new parameterizations that are specifically related to the process-based simulation of sediment availability, i.e., the bed interaction parameter, depth of disturbance, and soil drying time scale. The depth of disturbance and soil drying time scale could easily be replaced by process-based simulation as there is thorough knowledge on near-shore morphodynamics and beach hydrology. Moreover, the presented model framework allows for spatiotemporal variations of parameters that are known not to be constant (e.g., z'). However, these considerations are outside the scope of this paper and will be part of future research.

6.2. Calibration

The calibration of the parameters involved in process-based simulation of sediment availability is a relatively new field of research. In this paper a pragmatic approach to calibration of these parameters is adopted, but there are various opportunities for improvement. For example, the depth of disturbance is used to approximate the mixing of the intertidal beach surface by waves. *Masselink et al.* [2007] shows how the depth of disturbance can be determined based on a linear relation with the local wave height. The mixing of the intertidal beach surface is particularly important as it breaks beach armoring. The depth of disturbance does not provide any information about how the bed is disturbed, just over which depth. Moreover, aspects like marine deposits and shell buoyancy also affect the sediment availability in the intertidal beach area. *Gallagher et al.* [2011] presented detailed measurements of spatiotemporal variations in the bed surface grain size at Truc Vert, France. The intertidal beach appears to be consistently finer than the upper beach. The measurements are obtained using macrophotography [*Buscombe et al.*, 2010] ensuring that the measurements solely involve the beach surface. These type of measurements may provide a much more detailed calibration of the hydraulic mixing simulated in the model, although it might be questioned if such detailed hydraulic calibration is still within the scope of an aeolian sediment transport model. Alternatively, the calibration of the hydraulic mixing could be left to dedicated near-shore models (e.g., XBeach) [*Roelvink et al.*, 2009; *Reniers et al.*, 2013], and online model coupling could be used to incorporate detailed near-shore hydrodynamics and morphodynamics in the proposed aeolian modeling framework.

Similarly, an exponential decay function with a constant drying time scale is currently used to approximate the influence of the hydrological process of infiltration. The exponential decay is a simplified approach that was adopted after it appeared to be a reasonable approximation of numerical model results obtained with the HYDRUS model [*Šimůnek et al.*, 1998] that simulates the soil moisture contents in the unsaturated zone

following *van Genuchten* [1978]. Detailed measurements for calibration of the instantaneous soil moisture can be obtained relatively easy using either in situ or remote infrared or microwave measurements [e.g., *Edwards et al.*, 2013; *Hoonhout et al.*, 2014]. Again, it might be questioned if the amount of detail involved in using these kind of data for estimates of the bed surface moisture is still within the scope of an aeolian sediment transport model.

In contrast to the depth of disturbance and the drying rate, the bed interaction parameter has little relation with existing literature. In essence, the bed interaction parameter describes the exchange of momentum between grain size fractions along the fetch distance. Specifically, it describes whether impacting grains eject other grains from the bed or that they are rebounded due to fully elastic collisions with large, nonerodible elements. A low value for the bed interaction parameter would indicate a large number of rebounding grains, while a high value would indicate a low number of rebounding grains. Typically, the number of rebounded grains increases with an increasing number of nonerodible large elements in the bed. Consequently, the bed interaction parameter is not uniform over the fractions. Moreover, due to beach armoring the bed interaction is neither constant over time nor in space. In this paper the bed interaction parameter is pragmatically assumed to be uniform and constant since no basis for differentiation of the parameter is currently available. Thorough calibration of the bed interaction parameter would require detailed, spatiotemporal measurements of grain size distributions in the bed and the saltation cascade. It would require a series of sediment traps along the fetch that are regularly emptied and sieved as to determine the change of the grain size distribution in the saltation cascade in space and over time. Concurrently, the grain size distribution at the bed surface over the entire fetch needs to be monitored without disturbing the bed significantly. In a laboratory environment the change in grain size distribution could be monitored using sediment that is colored per fraction. Visual observation of the change in coloring then provides insight in the change in grain size distribution. However, the experiment should be performed at such scale that the trapping of sediment by upwind traps does not significantly influence the saltation cascade downwind over the period that the armor layer develops.

6.3. Validation

Validation of the proposed model is ongoing. Initially, validation will be focused on gross sediment transport rates in availability-limited systems. Few holistic measurements are available that monitor both the spatiotemporal variations in the sediment transport rate and the availability-limiting factors like moisture content and beach armoring concurrently [e.g., *Delgado-Fernandez et al.*, 2012; *Hoonhout et al.*, 2013]. Sites with detailed and frequent topographic measurements and hydrodynamic boundary conditions available can be found worldwide. These sites would be a good starting point for assessing the performance of the model compared to existing models. Using simplified, but generic descriptions of the hydraulic mixing and drying rate, the model should already provide time series of aeolian sediment transport that adhere much better to the true nature of aeolian sediment transport events than existing models. *Delgado-Fernandez and Davidson-Arnott* [2011] and *de Vries et al.* [2014b] already indicated that the true nature of these events is related not solely to wind velocity and direction but also to surges, seasons, spring/neap cycles, rain showers, and other events that influence sediment availability. The variations in aeolian sediment transport due to these event-driven changes in sediment availability are not well captured by models that rely solely on the wind transport capacity. The model has added value if it improves the prediction of transport rates under such circumstances.

7. Conclusions

The AEOLIS model presented in this paper is the first aeolian sediment transport model that simulates spatiotemporal variations in bed surface properties and sediment availability. Simulation of sediment availability is necessary as sediment availability cannot be determined a priori due to its recurrence relation with sediment transport. The presented model approach is a generalization of existing modeling concepts for aeolian sediment transport that include the influence of bed surface properties and limitations in sediment availability, like the shear velocity threshold and critical fetch, and is compatible with these concepts. The model uses an advection scheme following *de Vries et al.* [2014a] and a bed composition module that discretizes the bed in horizontal grid cells and vertical bed layers to account for spatial variations in bed surface properties. Temporal variations in sediment availability are not parameterized, but simulated using the bed composition module. The simulation of sediment availability reduces the need for complex spatiotemporal parameterizations and consequently calibration. In this paper the influence of sediment sorting and beach armoring and the reversed process of hydraulic mixing on aeolian sediment transport are illustrated using four prototype

cases. The model can reproduce patterns in aeolian sediment availability and transport as observed in wind tunnel experiments that involve spatiotemporal variations in bed surface properties [*Nickling and McKenna Neuman*, 1995; *Dong et al.*, 2004a]. Further, the model provides a generic framework to incorporate additional spatiotemporal varying processes that either influence sediment availability or the wind transport capacity with a minimum of parameterization. The framework allows relatively straightforward implementation of the effects of infiltration, evaporation, vegetation, buildings, and morphological feedback with the wind.

From this paper the following conclusions can be drawn:

1. A model for aeolian sediment transport was presented that simulates the processes of sediment sorting and beach armoring, the reversed process of hydraulic mixing, interaction between sediment fractions in the air with sediment fractions in the bed, and thereby the influence of spatiotemporal variations in sediment availability;
2. The model can be seen as a generalization of existing approaches to incorporate limitations in sediment availability and the wind transport capacity in aeolian transport estimates and is compatible with approaches based on either shear velocity thresholds or critical fetch;
3. The process of beach armoring can be a governing factor in aeolian sediment transport modeling and may reduce the estimated transport rates significantly and up to 95.0% in the presented prototype cases;
4. The model can reproduce typical patterns in aeolian sediment transport with spatiotemporal variations in sediment availability obtained from measurements from the unrelated wind tunnel experiments described in *Nickling and McKenna Neuman* [1995] and *Dong et al.* [2004a], with a minimum parameterization and calibration.

Acknowledgments
For their work discussed in this paper the authors are supported by the ERC-Advanced grant 291206—Nearshore Monitoring and Modeling (NEMO). The AEOLIS model described in this paper is available as open-source software through the OPENEARTH GIT repository https://github.com/openearth/aeolis-python. Results presented in this paper are obtained using the first release of the model published in *Hoonhout* [2016a] and using the model setups published in *Hoonhout* [2016b], both as GIT repositories.

References

Aagaard, T. (2014), Sediment supply to beaches: Cross-shore sand transport on the lower shoreface, *J. Geophys. Res. Earth Surf.*, *119*, 913–926, doi:10.1002/2013JF003041.

Arens, S., J. Van Boxel, and J. Abuodha (2002), Changes in grain size of sand in transport over a foredune, *Earth Surf. Processes Landforms*, *27*(11), 1163–1175.

Arens, S. M. (1996), Patterns of sand transport on vegetated foredunes, *Geomorphology*, *17*, 339–350.

Bagnold, R. (1935), The movement of desert sand, *Geogr. J.*, *85*, 342–365.

Bagnold, R. (1937), The transport of sand by wind, *Geogr. J.*, *89*, 409–438.

Bauer, B. O., and R. G. D. Davidson-Arnott (2002), A general framework for modeling sediment supply to coastal dunes including wind angle, beach geometry, and fetch effects, *Geomorphology*, *49*, 89–108, doi:10.1016/S0169-555X(02)00165-4.

Bauer, B. O., R. G. D. Davidson-Arnott, P. A. Hesp, S. L. Namikas, J. Ollerhead, and I. J. Walker (2009), Aeolian sediment transport on a beach: Surface moisture, wind fetch, and mean transport, *Geomorphology*, *105*, 106–116, doi:10.1016/j.geomorph.2008.02.016.

Belly, P. Y. (1964), Sand movement by wind, Tech. Rep. 1, 38 pp., U.S. Army Corps of Engineers CERC, Vicksburg, MS.

Buscombe, D., D. M. Rubin, and J. A. Warrick (2010), A universal approximation of grain size from images of noncohesive sediment, *J. Geophys. Res.*, *115*, F02015, doi:10.1029/2009JF001477.

Cheng, H., C. Liu, X. Zou, J. Li, J. He, B. Liu, Y. Wu, L. Kang, and Y. Fang (2015), Aeolian creeping mass of different grain sizes over sand beds of varying length, *J. Geophys. Res. Earth Surf.*, *120*, 1404–1417, doi:10.1002/2014JF003367.

Darke, I., and C. McKenna Neuman (2008), Field study of beach water content as a guide to wind erosion potential, *J. Coastal Res.*, *24*(5), 1200–1208, doi:10.2112/00-000.1.

Davidson-Arnott, R. G., D. C. White, and J. Ollerhead (1997), The effects of artificial pebble concentrations on eolian sand transport on a beach, *Can. J. Earth Sci.*, *34*(11), 1499–1508.

Davidson-Arnott, R. G. D., and B. O. Bauer (2009), Aeolian sediment transport on a beach: Thresholds, intermittency, and high frequency variability, *Geomorphology*, *105*, 117–126, doi:10.1016/j.geomorph.2008.02.018.

Davidson-Arnott, R. G. D., K. MacQuarrie, and T. Aagaard (2005), The effect of wind gusts, moisture content and fetch length on sand transport on a beach, *Geomorphology*, *68*, 115–129, doi:10.1016/j.geomorph.2004.04.008.

Davidson-Arnott, R. G. D., Y. Yang, J. Ollerhead, P. A. Hesp, and I. J. Walker (2008), The effects of surface moisture on Aeolian sediment transport threshold and mass flux on a beach, *Earth Surf. Processes Landforms*, *33*(1), 55–74, doi:10.1002/esp.1527.

de Vries, S., J. S. M. van Thiel de Vries, L. C. van Rijn, S. M. Arens, and R. Ranasinghe (2014a), Aeolian sediment transport in supply limited situations, *Aeolian Res.*, *12*, 75–85, doi:10.1016/j.aeolia.2013.11.005.

de Vries, S., S. M. Arens, M. A. de Schipper, and R. Ranasinghe (2014b), Aeolian sediment transport on a beach with a varying sediment supply, *Aeolian Res.*, *15*, 235–244, doi:10.1016/j.aeolia.2014.08.001.

Delft3D-FLOW Manual (2014), *Delft3D—3D/2D Modelling Suite for Integral Water Solutions—Hydro-Morphodynamics, Version 3.15.34158*, Deltares, Delft, Netherlands.

Delgado-Fernandez, I. (2010), A review of the application of the fetch effect to modelling sand supply to coastal foredunes, *Aeolian Res.*, *2*, 61–70, doi:10.1016/j.aeolia.2010.04.001.

Delgado-Fernandez, I., and R. A. Davidson-Arnott (2011), Meso-scale aeolian sediment input to coastal dunes: The nature of aeolian transport events, *Geomorphology*, *126*(1), 217–232, doi:10.1016/j.geomorph.2010.11.005.

Delgado-Fernandez, I., R. Davidson-Arnott, B. O. Bauer, I. J. Walker, J. Ollerhead, and H. Rhew (2012), Assessing aeolian beach-surface dynamics using a remote sensing approach, *Earth Surf. Processes Landforms*, *37*(15), 1651–1660, doi:10.1002/esp.3301.

Dong, Z., H. Wang, X. Liu, and X. Wang (2004a), A wind tunnel investigation of the influences of fetch length on the flux profile of a sand cloud blowing over a gravel surface, *Earth Surf. Processes Landforms*, *29*(13), 1613–1626, doi:10.1002/esp.1116.

Dong, Z., H. Wang, X. Liu, and X. Wang (2004b), The blown sand flux over a sandy surface: A wind tunnel investigation on the fetch effect, *Geomorphology*, *57*, 117–127, doi:10.1016/S0169-555X(03)00087-4.

Dupont, S., G. Bergametti, and S. Simoëns (2014), Modeling aeolian erosion in presence of vegetation, *J. Geophys. Res.*, *119*, 168–187, doi:10.1002/2013JF002875.
Dyer, K. R. (1986), *Coastal and Estuarine Sediment Dynamics*, 342 pp., Wiley, Chichester, U. K.
Edwards, B. L., and S. L. Namikas (2009), Small-scale variability in surface moisture on a fine-grained beach: Implications for modeling aeolian transport, *Earth Surf. Processes Landforms*, *34*, 1333–1338, doi:10.1002/esp.1817.
Edwards, B. L., S. L. Namikas, and E. J. D'Sa (2013), Simple infrared techniques for measuring beach surface moisture, *Earth Surf. Processes Landforms*, *38*(2), 192–197, doi:10.1002/esp.3319.
Gallagher, E. L., J. MacMahan, A. Reniers, J. Brown, and E. B. Thornton (2011), Grain size variability on a rip-channeled beach, *Mar. Geol.*, *287*(1), 43–53, doi:10.1016/j.margeo.2011.06.010.
Gillette, D. A., and P. H. Stockton (1989), The effect of nonerodible particles on wind erosion of erodible surfaces, *J. Geophys. Res.*, *94*(D10), 12,885–12,893.
Gillies, J. A., W. G. Nickling, and J. King (2006), Aeolian sediment transport through large patches of roughness in the atmospheric inertial sublayer, *J. Geophys. Res.*, *111*, F02006, doi:10.1029/2005JF000434.
Hoonhout, B. M. (2016a), GIT Repository, vol.
Hoonhout, B. M. (2016b), GIT Repository, vol.
Hoonhout, B. M., S. de Vries, F. Baart, J. S. M. van Thiel de Vries, L. van der Weerd, and K. M. Wijnberg (2013), Monitoring of beach surface properties with remote sensing, in *Proceedings of Coastal Dynamics*, Arcachon, 821–832.
Hoonhout, B. M., F. Baart, and J. S. M. Van Thiel de Vries (2014), Intertidal beach classification in infrared images, *SI*, *66*, 657–662.
Hotta, S., S. Kubota, S. Katori, and K. Horikawa (1984), Sand transport by wind on a wet sand beach, in *Proceedings of the 19th Conference on Coastal Engineering*, pp. 1264–1281, ASCE, Houston, Tex.
Howard, A. D. (1977), Effect of slope on the threshold of motion and its application to orientation of wind ripples, *Geol. Soc. Am. Bull.*, *88*(6), 853–856, doi:10.1130/0016-7606(1977)88<853:EOSOTT>2.0.CO;2.
Hsu, S.-A. (1971), Wind stress criteria in eolian sand transport, *J. Geophys. Res.*, *76*(36), 8684–8686.
Iversen, J. D., and K. R. Rasmussen (2006), The effect of surface slope on saltation threshold, *Sedimentology*, *41*(4), 721–728, doi:10.1111/j.1365-3091.1994.tb01419.x.
Jackson, D. W. T., and J. A. G. Cooper (1999), Beach fetch distance and aeolian sediment transport, *Sedimentology*, *46*, 517–522, doi:10.1046/j.1365-3091.1999.00228.x.
Johnson, J. W. (1965), Sand movement on coastal dunes, Tech. Rep. 570, pp. 747–755, Symp. 3, Paper no. 75, U.S. Dep. of Agriculture, Washington, D. C.
Kawamura, R. (1951), Study of sand movement by wind, Hydraulics Engineering Laboratory, Univ. of California, Berkeley.
King, C. A. M. (1951), Depth of disturbance of sand on sea beaches by waves, *J. Sediment. Petrol.*, *21*(3), 131–140.
King, J., W. G. Nickling, and J. A. Gillies (2005), Representation of vegetation and other nonerodible elements in Aeolian shear stress partitioning models for predicting transport threshold, *J. Geophys. Res.*, *110*, F04015, doi:10.1029/2004JF000281.
Kocurek, G., and N. Lancaster (1999), Aeolian system sediment state: Theory and Mojave Desert Kelso dune field example, *Sedimentology*, *46*(3), 505–515, doi:10.1046/j.1365-3091.1999.00227.x.
Lancaster, N., and A. Baas (1998), Influence of vegetation cover on sand transport by wind: Field studies at Owens Lake, California, *Earth Surf. Processes Landforms*, *23*(1), 69–82.
Lettau, K., and H. Lettau (1978), Experimental and micrometeorological field studies of dune migration, in *Exploring the World's Driest Climate*, pp. 110–47, Center for Climatic Res., Univ. of Madison-Wisconsin.
Li, J., G. S. Okin, J. E. Herrick, J. Belnap, M. E. Miller, K. Vest, and A. E. Draut (2013), Evaluation of a new model of aeolian transport in the presence of vegetation, *J. Geophys. Res. Earth Surf.*, *118*, 288–306, doi:10.1002/jgrf.20040.
Lynch, K., D. W. T. Jackson, and J. A. G. Cooper (2008), Aeolian fetch distance and secondary airflow effects: The influence of micro-scale variables on meso-scale foredune development, *Earth Surf. Processes Landforms*, *33*(7), 991–1005, doi:10.1002/esp.1582.
Masselink, G., N. Auger, P. Russell, and T. O'Hare (2007), Short-term morphological change and sediment dynamics in the intertidal zone of a macrotidal beach, *Sedimentology*, *54*, 39–53, doi:10.1111/j.1365-3091.2006.00825.x.
McKenna Neuman, C., and W. Nickling (1995), Aeolian sediment flux decay: Non-linear behaviour on developing deflation lag surfaces, *Earth Surf. Processes Landforms*, *20*(5), 423–435.
McKenna Neuman, C., and S. Sanderson (2008), Humidity control of particle emissions in aeolian systems, *J. Geophys. Res.*, *113*, F02S14, doi:10.1029/2007JF000780.
McKenna Neuman, C., B. Li, and D. Nash (2012), Micro-topographic analysis of shell pavements formed by aeolian transport in a wind tunnel simulation, *J. Geophys. Res.*, *117*, F04003, doi:10.1029/2012JF002381.
Namikas, S. L., B. L. Edwards, M. C. A. Bitton, J. L. Booth, and Y. Zhu (2010), Temporal and spatial variabilities in the surface moisture content of a fine-grained beach, *Geomorphology*, *114*, 303–310, doi:10.1016/j.geomorph.2009.07.011.
Nickling, W., and C. McKenna Neuman (1995), Development of deflation lag surfaces, *Sedimentology*, *42*(3), 403–414.
Nickling, W. G., and M. Ecclestone (1981), The effects of soluble salts on the threshold shear velocity of fine sand, *Sedimentology*, *28*, 505–510.
Okin, G. S. (2008), A new model of wind erosion in the presence of vegetation, *J. Geophys. Res.*, *113*, F02S10, doi:10.1029/2007JF000758.
Owen, P. R. (1964), Saltation of uniform grains in air, *J. Fluid Mech*, *20*(2), 225–242.
Raupach, M., D. Gillette, and J. Leys (1993), The effect of roughness elements on wind erosion threshold, *J. Geophys. Res.*, *98*(D2), 3023–3029, doi:10.1029/92JD01922.
Reniers, A., E. Gallagher, J. MacMahan, J. Brown, A. Rooijen, J. Thiel de Vries, and B. Prooijen (2013), Observations and modeling of steep-beach grain-size variability, *J. Geophys. Res. Oceans*, *118*, 577–591, doi:10.1029/2012JC008073.
Roelvink, J. A., A. Reniers, A. P. van Dongeren, J. S. M. van Thiel de Vries, R. T. McCall, and J. Lescinski (2009), Modelling storm impacts on beaches, dunes and barrier islands, *Coastal Eng.*, *56*(11), 1133–1152, doi:10.1016/j.coastaleng.2009.08.006.
Scheidt, S., M. Ramsey, and N. Lancaster (2010), Determining soil moisture and sediment availability at white sands dune field, New Mexico, from apparent thermal inertia data, *J. Geophys. Res.*, *115*, F02019, doi:10.1029/2009JF001378.
Sherman, D. J., and B. Li (2012), Predicting aeolian sand transport rates: A reevaluation of models, *Aeolian Res.*, *3*(4), 371–378, doi:10.1016/j.aeolia.2011.06.002.
Sherman, D. J., D. W. Jackson, S. L. Namikas, and J. Wang (1998), Wind-blown sand on beaches: An evaluation of models, *Geomorphology*, *22*(2), 113–133, doi:10.1016/S0169-555X(97)00062-7.
Shuttleworth, W. J. (1993), Evaporation, in *Handbook of Hydrology*, edited by D. R. Maidment, pp. 4.1–4.53, McGraw-Hill, New York.
Sørensen, M. (2004), On the rate of aeolian sand transport, *Geomorphology*, *59*(1), 53–62.

Stout, J. E. (2004), A method for establishing the critical threshold for aeolian transport in the field, *Earth Surf. Processes Landforms*, *29*(10), 1195–1207.

Tan, L., W. Zhang, J. Qu, K. Zhang, Z. An, and X. Wang (2013), Aeolian sand transport over Gobi with different gravel coverages under limited sand supply: A mobile wind tunnel investigation, *Aeolian Res.*, *11*, 67–74, doi:10.1016/j.aeolia.2013.10.003.

Turpin, C., T. Badr, and J. L. Harion (2010), Numerical modelling of aeolian erosion over rough surfaces, *Earth Surf. Processes Landforms*, *35*(12), 1418–1429, doi:10.1002/esp.1980.

Udo, K., Y. Kuriyama, and D. W. T. Jackson (2008), Observations of wind-blown sand under various meteorological conditions at a beach, *J. Geophys. Res.*, *113*, F04008, doi:10.1029/2007JF000936.

van der Wal, D. (1998), The impact of the grain-size distribution of nourishment sand on aeolian sand transport, *J. Coastal Res.*, *14*, 620–631.

van der Wal, D. (2000), Grain-size-selective aeolian sand transport on a nourished beach, *J. Coastal Res.*, *16*, 896–908.

van Genuchten, M. T. (1978), Mass transport in saturated-unsaturated media: One-dimensional solutions, *Tech. Rep. Res. Rep. No. 78-WR-11*, Univ. Princeton, Water Resources Program.

Šimůnek, J., M. Šejna, and M. T. van Genuchten (1998), *The HYDRUS-1D Software Package for Simulating the One-Dimensional Movement of Water, Heat, and Multiple Solutes in Variably-Saturated Media*, version 1.0. igwmc–tps - 70 ed., 186 pp., International Ground Water Modeling Center, Colorado School of Mines, Golden, Colo.

Wiggs, G. F. S., A. J. Baird, and R. J. Atherton (2004), The dynamic effects of moisture on the entrainment and transport of sand by wind, *Geomorphology*, *59*, 13–30, doi:10.1016/j.geomorph.2003.09.002.

Williams, A. T. (1971), An analysis of some factors involved in the depth of disturbance of beach sand by waves, *Mar. Geol.*, *11*(3), 145–158, doi:10.1016/0025-3227(71)90003-X.